Proceedings of the Combustion Institute, Volume 29, 2002/pp. 1155–1163

PREDICTING NO_x EMISSIONS OF A BURNER OPERATED IN FLAMELESS OXIDATION MODE

MARCO MANCINI,[1] ROMAN WEBER[2] AND UGO BOLLETTINI[3]

[1]*International Flame Research Foundation*
Research Station B.V.
PO Box 10 000
1970 CA Ijmuiden, The Netherlands
[2]*Institut für Energieverfahrenstechnik und Brennstofftechnik der TU Clausthal*
Agricolastrasse 4
38678 Clausthal-Zellerfeld, Germany
[3]*ENEA Engineering Division*
CR Casaccia—Via Anguillarese, 301
00060 S.M. di Galeria, Rome, Italy

This paper deals with the technology of burning natural gas with combustion air preheated to 1300 °C. The objective of this work is to assess the potential of several combustion models and NO_x postprocessors for their abilities to predict NO_x emissions. The steady-state computational results have been compared both with in-furnace measurements and with the measured furnace exit parameters. The following main conclusions have been drawn: (1) with the exception of the small region located within the natural gas jet, the computations resulted in good quality predictions; (2) the NO_x has been formed in a thin elongated region (flamelet) located between the natural gas jet and the air jet; (3) the NO has been formed mainly by the thermal path, and the NO-reburning mechanism was of little importance; and (4) there are strong indications that the non-stationary behavior of the weak (fuel) jet must be accounted for if the predictions within the fuel jet were to be perfected.

Introduction

Combustion of fuels with high-temperature air and large quantities of flue gas is perhaps the most rapidly developing combustion technology of the past decade [1–3]. The technology, when applied together with an efficient heat recovery system, offers substantial energy savings and drastic reductions in CO_2, CO, and NO_x emissions. Initially, the technology was named in Japan as excess enthalpy combustion, the term used by Hardesty and Weinberg [4] to describe burners with heat recycling. Later on it was renamed high-temperature air combustion (HTAC). In Italy, the process has been named mild combustion [5], while in the United States, the term low-NO_x injection is used. In Germany, the process has been called flameless oxidation [3].

There are different methods of realization of this combustion technology. However, two of them seem to be widely applied. The flameless oxidation burner [3] possesses a central jet of natural gas and a number (typically 6 or 12) of air jets supplying preheated combustion air. The combustion air jets are spaced around the central natural gas jet. Before mixing with the natural gas jet, the air jets entrain large quantities of the recirculated combustion products. Thus, the fuel is oxidized in combustion products containing some oxygen (typically not more than 5%). In Japanese designs [6], in IFRF designs [2], the preheated air is supplied through a central jet, whereas natural gas is provided by several injectors located on the circumference of the burner (see also Ref. [7]). The natural gas injectors are positioned away from the air jet so as to inject the fuel into hot combustion products that contain 1%–2% oxygen. The natural gas jets do not mix with the air stream until further downstream in the furnace, and by that time (distance), the fuel jets are substantially diluted with combustion products. In both flameless oxidation burners and combustion systems with fuel injectors positioned away from the air jet, the fuel gas is oxidized in an environment that contains a substantial amount of inert gases (N_2,CO_2,H_2O) and some, typically not more than 5%, oxygen. In this respect, both modes of combustion are similar. In most industrial applications, burners are used in pairs with a firing cycle of 20–50 s due to the built-in heat regenerators or recuperators.

There has been relatively little support of the fundamental combustion community to provide the adequate scientific insight, as pointed out in Refs. [1,2]. Mathematical modeling of flameless oxidation has received little attention. The first modeling efforts originated from Japanese industry [8,9]. They show

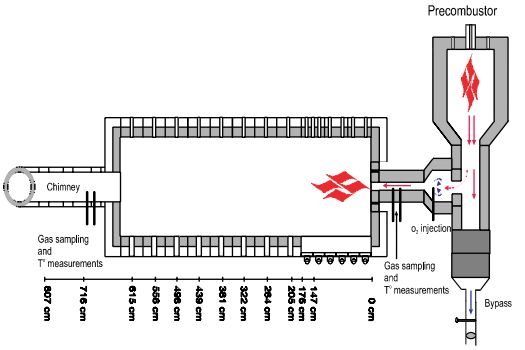

FIG. 1. Experimental furnace.

that numerical codes based on the mixture-fraction/probability density function (pdf) approach are able to describe the main characteristics in terms of the flow and temperature fields of high air temperature combustion. However, they found that the present NO_x models might require improvement to describe properly the NO_x formation under low-temperature conditions. In the above-cited work, the assessment of the model performance was made exclusively on the basis of comparing the predictions with the measured furnace exit values since no in-furnace data were available. Furthermore, although the burners operated in cycles, the predictions were carried out under steady-state conditions.

More recently, Coelho and Peters [10] carried out numerical simulations of a mild combustion (FLOX) burner that operated at 10 kW thermal input with a relatively low level of air preheat (500 °C). The experimental furnace was operated at a rather low temperature of 1000 °C, resulting in NO_x emissions around 10 ppm. Coelho and Peters [10] argued that the steady flamelet library was unable to "correctly describe the formation of NO since this is a chemically slow process, which is sensitive to transient effects" while the unsteady flamelet model was able to predict "the correct order of magnitude of NO emissions." Also in this case, the conclusions were drawn on the basis of the comparison of the predictions with the furnace exit values since limited in-furnace measurements were available. Another interesting paper was published at the time of preparing of this paper. Pasenti et al. [11] undertook a task of simulating a 200 kW FLOX burner operated under cyclic (unsteady state) conditions. The furnace exit temperature was varied in the range 1090–1330 °C (using a heat sink) resulting in NO_x emissions that increased (with the furnace exit temperature) from 4 to 40 ppm (at 3% O_2). The steady-state numerical simulations [11] resulted in good predictions of the total radiative heat flux. The NO_x emissions were substantially underpredicted although the dependence (trend) of the NO_x emissions on the furnace exit temperature was correctly represented in the predictions.

It is apparent that there is a lack of in-furnace data corresponding to flameless oxidation, and consequently the mathematical modeling is speculative. It is extremely difficult to generate such data under non-stationary conditions that are typical of industrial applications of flameless oxidation combustion. To the best of the authors' knowledge, there is only one set of in-furnace data collected under steady-state conditions that contains the in-furnace measured temperatures, velocity field, chemistry field (O_2,CO,CO_2, H_2, CH_4, NO_x, NO) and radiative fluxes. In 1997, the IFRF [2] generated such data. We have used [12] the IFRF data to develop and validate models for predicting the flow field (including jet entrainments), temperature field, and chemistry field (O_2, CO_2, CO, H_2O, unburned hydrocarbons). In this publication, we focus exclusively on predicting NO_x emissions. Later on, we will demonstrate that our steady-state calculations result in excellent NO predictions for conditions of high air preheat (1300 °C) and high furnace exit temperature (1222 °C) and for a steady-state operation of a natural gas burner at 0.58 MW fuel input.

Objectives

The objective of our work is to develop and validate a mathematical model for predicting combustion characteristics, including NO_x emissions, of flameless combustion of natural gas, since the conditions of uniform and low-temperature and low-O_2 concentration are substantially different from those encountered in conventional burner technology. We wish to identify the location of regions of NO_x formation and establish how important are the NO_x reburning mechanism and prompt-NO formation mechanism.

Experimental

The semi-industrial scale experiments [2] were carried out in a refractory lined furnace with a 2 × 2 m cross-section and a length of 6.25 m, (Fig. 1).

The furnace was equipped with only one burner operated under steady-state conditions. The high-temperature regenerator was replaced by a precombustor where natural gas was burned with air under lean conditions. Oxygen was added to the hot gases leaving the precombustor to maintain its concentration at 21%. Such a comburent simulated the air preheat of the excess enthalpy combustion process. The experimental burner (see Fig. 2 of Ref. [12]) was a 1:1 copy of NFK burner that operated at 0.58 MW fuel input and the combustion air was preheated to 1300 °C.

TABLE 1
Experimental conditions

	Flow rate (kg/h)	Temp. (°C)	Enthalpy (MW)	Composition % (vol)
Natural gas	47	25	0.58	CH_4 87.8%, C_2H_6 4.6%, C_3H_8 1.6%, C_4H_{01} 0.5%, 5.5% N2; LCV = 44.76 MJ/kg
Comburent	830	1300	0.35	19.5% wet O_2, 59.1% wet N_2, 15% H_2O, 6.4% wet, CO_2, NO 110 ppm vd
Furnace exit gases	877	1220	0.380	1.6% wet O_2, 140 ppm vd NO_x

The comburent was supplied through the central channel with an injection velocity of ~85 m/s. The natural gas injectors were located 280 mm away form the burner centerline. The fuel was supplied through two injectors with an injection velocity of ~100 m/s. The input-output conditions of the experiment are listed in Table 1.

During the test, the flue gas temperature and flue gas compositions were continuously monitored using a suction pyrometer and a gas sampling probe. Under steady operating conditions, a complete set of in-flame measurements was acquired, including the flow and mixing patterns, the total radiative heat flux, and the combustion gas temperatures and gas composition. Detailed mapping of the turbulent velocities was carried out using laser doppler velocimetry (LDV). The in-furnace temperatures were measured using a suction pyrometer, while the furnace wall temperatures were obtained using type B thermocouples. A cranked probe, operated under quenching rate of 10^7–10^8 K/s, was used to sample the gas which was analyzed for oxygen, carbon monoxide, carbon dioxide, methane, hydrogen, and nitric oxides. An ellipsoidal radiometer was used to measure hemispherical fluxes at the furnace wall. The in-furnace measurements, reported in this paper, were obtained by traversing the furnace in the horizontal plane of the two fuel injectors [2].

Mathematical Models

Combustion Models

In the present study, three different combustion models were applied to simulate natural gas combustion with high-temperature air:

- An eddy break-up (EBU)–mixed-in burned model
- An eddy dissipation (EDC)–chemical equilibrium model
- A mixture fraction/pdf model (PDF) with equilibrium look-up tables.

Due to the lack of space, only a short description of the applied models is given here and the reader is requested to consult the original papers. The IFRF EBU combustion model [13] considers six major chemical species: hydrocarbons (C_xH_y), oxygen, carbon monoxide, carbon dioxide, water vapor, and nitrogen. The combustion is modeled with a two-step reaction scheme. The hydrocarbon C_xH_y, is first oxidized to CO and H_2O, while intermediate CO oxidizes to CO_2. The various source and sink terms entering the chemical species mass balance equation are described using the eddy break-up model of Magnussen and Hjertager [14]. The eddy break-up model makes use of a proportionality constant, the mixing rate coefficient, that is calculated in each numerical cell as a function of the local Reynolds number [13].

The EDC model of Magnussen [15] is derived using a detailed description of the dissipative process in the flow. The model derivation starts with the expressions describing the dissipation of turbulent kinetic energy. Further on, characteristic velocity and length scales for turbulent structures where the mixing is completed are derived. In the EDC, these turbulent structures are called fine structures. Using the velocity scale and length scale associated with the fine structures, an expression for calculating the mass transfer rate between the surrounding and the fine structure is derived. The chemical composition within the fine structures is obtained by solving a perfectly stirred reactor problem using the thermodynamic equilibrium approach. The equilibrium composition was calculated using the CEA code of NASA and 13 species were considered: C_2H_6, CH_4, CO_2, O_2, H_2O, H_2, H, OH, O, NO, NO_2, and N_2. The model used here is identical to the one used by Brink et al. [16] and Orsino at al. [12].

The third model is the mixture fraction model combined with the β-probability density function to handle the fluctuations. The β-function PDF shape is calculated from the mean mixture fraction and its variance. An additional transport equation for the variance of the mixture fraction is solved. The computational time is optimized using a preprocessor to obtain the equilibrium composition of all the chemical species considered in the calculations. During the preprocessing three-dimensional look-up tables

are generated for the mean flame temperature, density, and species mole fraction as a function of the mean mixture fraction, its variance, and the enthalpy. In the present work, 11 chemical species (CH_4, C_2H_6, C_3H_8, C_4H_{10}, CO, CO_2, H_2O, OH, N_2, O_2, and H_2) have been considered. While for the EBU and the EDC, the IFRF software was used, the Fluent CFD code (version 5.4) was used to run the PDF model.

NO_x Postprocessors

Chemical reaction rates of NO formation and NO concentrations are postcalculated using previously computed velocities, turbulence, temperature, and chemistry fields. In the combustion of natural gases, the two principal formation mechanisms of NO are oxidation of molecular nitrogen (thermal-NO formation) and the mechanism in which hydrocarbon radicals attack molecular nitrogen to form nitrogen radicals, the latter subsequently reacting with the molecular oxygen to form NO (prompt-NO formation). In fuel-rich regions, NO can be reduced by CH_i radicals to form species like HCN, which subsequently produces NO or N_2. This reduction mechanism is known as NO-reburning mechanism or fuel-staging mechanism.

IFRF NO_x model

Thermal NO and prompt NO are calculated in the same way as in Ref. [13] with no changes to any of the model parameters and constants. However, we added the NO-reburning path following the work of Chen [17] and De Soete [18]:

$$\mathrm{NO} + \mathrm{C}_x\mathrm{H}_y \rightarrow \mathrm{HCN} + \ldots \qquad \text{(R9)}$$

$$\mathrm{HCN} + \mathrm{O}_2 \rightarrow \mathrm{NO} + \ldots \qquad \text{(R10)}$$

$$\mathrm{HCN} + \mathrm{NO} \rightarrow \mathrm{N}_2 + \ldots \qquad \text{(R11)}$$

It might be useful to note that in light of the present knowledge of NO precursors kinetics, the famous CH + N_2 reaction does not go to NCN and N as products, but rather the NCN + H reaction. Hence, the sequence of reactions R9 + R10, proposed by Chen [17], and used in this study, does not have a firm basis in kinetics, as we now understand them.

For reaction R9, Chen [17] proposes the rate

$$r_{9-\mathrm{NO}} = 2.68 * 10^6\ [\mathrm{C}_x\ \mathrm{H}_y]\ [\mathrm{NO}]\ \exp\left(-\frac{18{,}900}{RT}\right)$$

For reactions 10 and 11, De Soete [18] proposes

$$r_{10-\mathrm{NO}} = 10^{10}\left(\frac{M_{\mathrm{mix}}}{\rho_{\mathrm{mix}}}\right)^b [\mathrm{HCN}]\ [\mathrm{O}_2]^b \exp\left(-\frac{67{,}000}{RT}\right)$$

$$r_{11-\mathrm{NO}} = 3 \cdot 10^{12}\left(\frac{M_{\mathrm{mix}}}{\rho_{\mathrm{mix}}}\right) [\mathrm{HCN}]\ [\mathrm{NO}] \exp\left(-\frac{60{,}000}{RT}\right)$$

where M_{mix} and ρ_{mix} are the mixture molecular weight and the mixture density, respectively. The power b is locally calculated according to De Soete [18]:

$$b = -1.4799 - 1.4593c - 0.4859c^2 - 0.0546c^3, \quad c = \ln\left(\frac{M_{\mathrm{mix}}}{M_{\mathrm{o_2}}}\ [\mathrm{O}_2]\right)$$

The interaction between turbulent flow and chemistry is taken into account through the transport equation of NO chemical species. The source term of this equation, which is the time-mean chemical reaction rates of NO formation/reduction, is computed on the basis of the single-variable pdf model. Since the formation and reduction mechanisms of NO are strongly temperature-dependent, a presumed, single-variable pdf approach has been chosen. For the instantaneous gaseous phase temperature, T, the β-pdf $\beta_{\mathrm{pdf}}(T; a,b)$ has been chosen. The time-mean rates of thermal NO, prompt NO, and NO reburning are approximated by the expectations $\mathrm{Exp}(r_{k-\mathrm{NO}})$ of the original chemical reaction rates $r_{k-\mathrm{NO}}$.

$$r_{k-\mathrm{NO}} = \mathrm{Exp}\,(r_{k-\mathrm{NO}}) = \int_{T_u}^{T_b} r_{k-\mathrm{NO}}\,(T)\beta_{\mathrm{pdf}}\,(T; a,b)\,\frac{dT}{T_{\mathrm{b}} - T_{\mathrm{u}}}, \quad k = t,\ p,\ r$$

Nitric oxide models used with the pdf combustion model

The NO_x postprocessing used with the pdf/combustion models considers the thermal and prompt mechanisms. The NO_x-reburning mechanism is excluded. The extended Zeldovich mechanism is used, and the rate constants are taken from Hanson and Salimian [19] The prompt NO_x mechanism is modeled following the overall simplified NO-formation rate proposed by the De Soete [18]. The interactions with the turbulence are predicted using a pdf approach using a β-function. The limits of the pdf integration are determined from the maximum and minimum values of the predicted temperature in the computational domain. The Fluent CFD code (version 5.4) is used in this paper to run the NO_x postprocessor described in this paragraph.

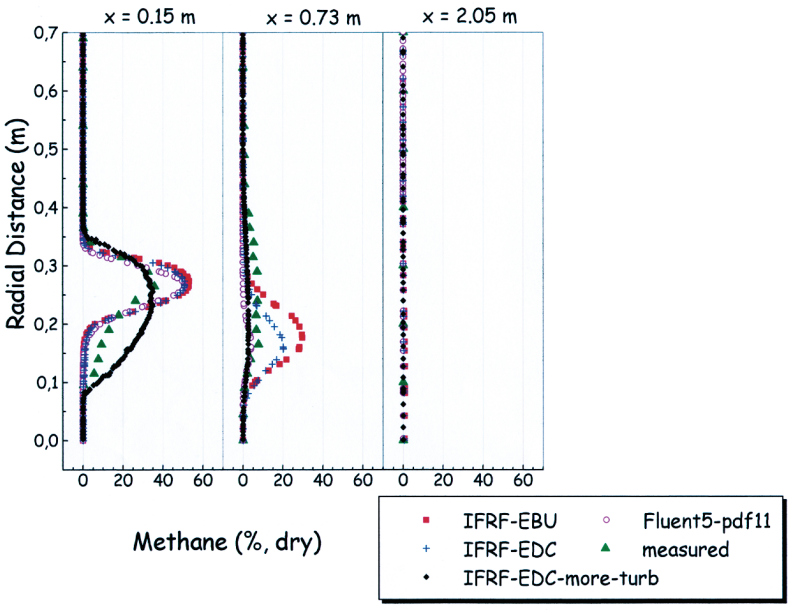

FIG. 2. Measured and predicted methane concentrations.

Results

The experimental furnace had two symmetry planes; therefore, a grid reproducing only one-quarter of the furnace was built. The grid was a structured hexahedral mesh of the geometrical domain with 92 × 42 × 129 (498, 456) cells. The flow field has been calculated using the k-ϵ model of turbulence. The furnace exit parameters have been predicted with a very good accuracy. For example, a temperature of 1493 K was measured while the predicted values were 1522, 1531, and 1521 K for the EBU, Fluent5-pdf, and EDC models, respectively. A concentration of 2.5% O_2 was calculated for all the models.

Prior to carrying out an assessment of the NO_x processors, it is imperative to identify the imperfections in the computed in-furnace temperature and oxygen. Fig. 2 shows the unburned methane concentrations, while the measured and predicted time mean temperatures are shown in Fig. 3. In these figures, zero radial distance represents the furnace centerline (comburent injection), and the natural gas injection is located at 0.28 m radial distance. For the time being, we shall concentrate on the predictions obtained with the EBU model (marked in Figs. 2 and 3 as IFRF-EBU), the EDC model (marked as IFRF-EDC), and the pdf model (marked as Fluent5-pdf11). Later on, we will consider the predictions marked in Figs. 2 and 3 as IFRF-EDC-more-turb. The figures demonstrate the following (predictions of the velocities, O_2, CO, radiative heat fluxes, and the furnace wall temperature can be found in Ref. [12]):

1. The numerical models have correctly reproduced the uniformity of the temperature field and the oxygen field. All the three combustion models provided the predictions of similar quality. The EDC model and the pdf/mixture fraction model when coupled with chemical equilibrium have provided very similar results.
2. The three tested combustion models cannot describe the chemistry and temperature field in the fuel jet region.

The temperatures in the fuel jet are determined by the rate of energy release (due to combustion) and the rate of entrainment of hot combustion products into the jet. The oxygen needed for methane combustion is entrained into the jet from the surroundings. All three models underestimated the rate of methane consumption as shown in Fig. 2. The predicted entrainment into the fuel jet was by a factor of 2 lower than the measured one (computational runs with the realizable k-ϵ turbulence model or the Reynolds stress model offered marginal changes). Our analysis of jet entrainment [12] has shown that even correcting for the entrainment would not result in the temperature increase that would fully compensate for such a large difference between the measured and the predicted temperatures within the methane jet. The questions we wish to address are: What is the reason for the failure of all the models in the fuel jet region? What are the consequences of

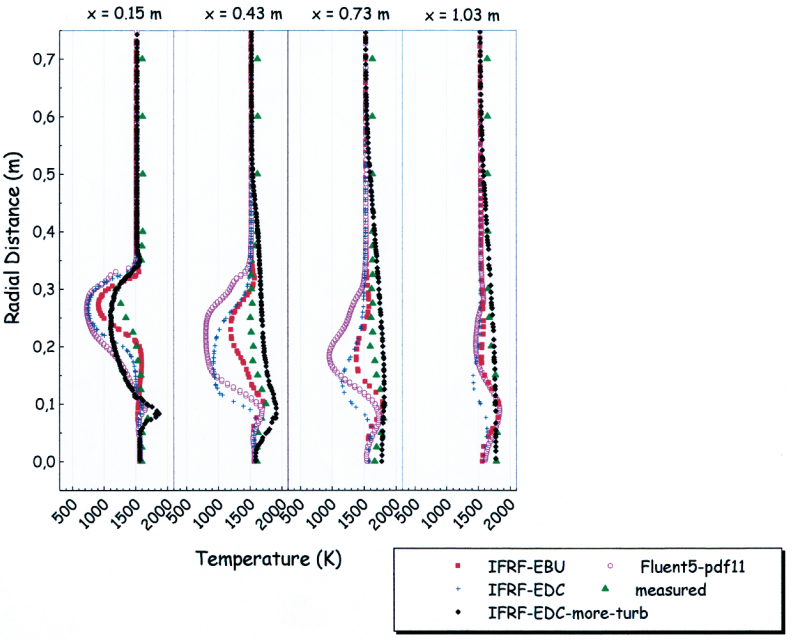

FIG. 3. Measured and predicted temperatures.

TABLE 2
Measured and predicted NO_x emissions at the furnace exit

Combustion model	NO_x model	Predictions (ppm, dry)		
		Total[a]	Thermal[a]	Prompt[a]
IFRF-EBU	IFRF	137	130	9
IFRF-EDC	IFRF	132	130	6
Fluent5-pdf (temp)	Fluent5	150	147	7
Fluent5-pdf (mixture fraction)	Fluent5	130	127	5
IFRF-EDC-more turbulence	IFRF	132	130	6

Note: Measurements: Inlet NO_x (in comburent), 110 ppm, dry; furnace exit NO_x, 140 ppm, dry.

[a] In column Total, the predicted furnace NO concentration is listed. The predictions are obtained with both thermal-NO and prompt-NO submodels activated and the inlet NO is 110 ppm, dry. Column Thermal lists the predictions when only the thermal-NO submodel is activated and the inlet NO (in comburent) is 110 ppm, dry. Column Prompt refers to the computational run with only prompt-NO submodel activated and nil NO inlet concentration.

the failure with respect to the NO_x emissions predictions? We begin with the second question.

NO_x Emissions

The same NO_x model (described above) was used with the EDC and EBU combustion model. Thus, the differences in the NO_x predictions between these two cases are solely due to differences in the temperature and chemistry fields. The second NO_x model (described above) was used as the postprocessor to the pdf-predicted temperature and chemistry fields. Two options were used here, one with the temperature variance calculations and the second one with the mixture fraction variance calculations. Table 2 reports the comparison of the measured and predicted NO_x emissions. While comparing the measurements and the predictions it should be remembered that a large part of the furnace exit NO_x was coming from the comburent that contained 110 ppmvd NO_x. Relatively little net NO_x generation (0.8 mg/s) was observed in the measurements if compared to the amount (24 mg/s) of NO that entered the furnace with the comburent. All the NO_x submodels performed well, and the predicted

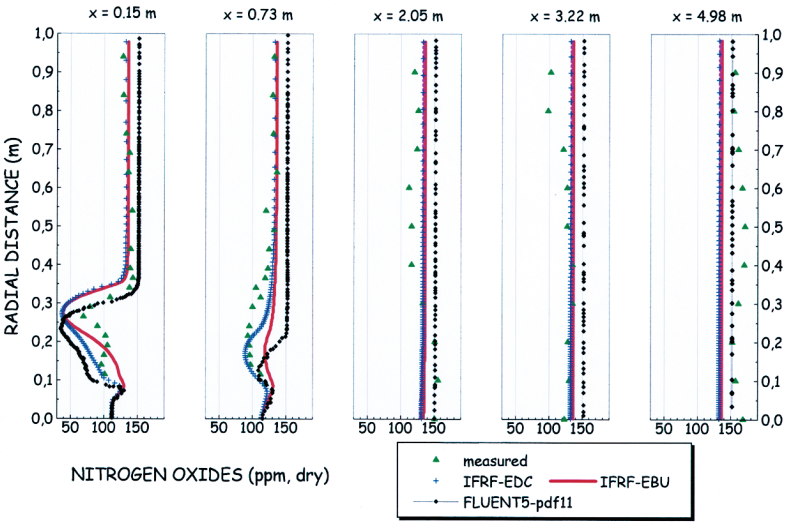

FIG. 4. Measured and predicted NO_x concentrations ppm, vol, dry. The predictions marked as Fluent5-pdf11 case were obtained using the equation for temperature variance transport (see Table 2).

net NO_x generation was very much in agreement with the measurements. An additional computational run, using the IFRF-EDC model in combination with the NO_x) submodel described above, was made with the inlet (comburent) NO_x level set to nil. The run resulted in 28 ppm NO_x at the furnace exit.

Figure 4 shows the measured and predicted in-furnace NO_x concentrations. The peak in the NO_x concentration was at the boundary of the air and natural gas jet where the highest temperature were both measured and predicted. The predictions were able to capture well this behavior. The NO_x concentration showed a peak between the air jet and the fuel jet at the two first traverses. The source of the NO_x (net) formation rate was located in this thin, elongated region (flamelet) between the air and the fuel jet. The NO net formation rates were several orders of magnitude lower than in conventional burner technology [13]. Using the EBU and the EDC combustion models the influence of the NO_x-reburning mechanism was investigated. The NO_x reduction rates were 4–5 orders of magnitude lower than the NO_x formation rates. Additional computational runs were made with the thermal-NO and prompt-NO submodels deactivated (see Table 2) showing that around 95% of the furnace exit NO was formed via the thermal path.

The Fuel Jet

We have already observed substantial differences between the predicted and the measured temperatures (Fig. 3) in the fuel jet, irrespectively of the combustion model used. Furthermore these differences seemed to be of little importance as far as the NO_x predictions were concerned. The applications of more sophisticated turbulence models (see above) brought little changes, and no substantial changes were observed when the kinetic turbulence energy at the inlet of the fuel jet was increased by a factor of three. This was so, since the inlet kinetic energy was rapidly dissipated before the fuel jet entered the furnace (the computations originated at 100 mm upstream of the furnace front wall; see Fig. 1). We should recall that our computations were carried out under steady-state conditions, thus, as if the (weak) fuel jets were stiff and straight. The laser sheet visualization applied during the measurements show the fuel jets dancing around while the central strong (comburent) jet remained straight and stiff. This observation would suggest that unless these non-stationary effects are accounted for, there would be a little chance of success in predicting the fuel jet properties. Figs. 2 and 3 show an additional computational run (marked IFRF-EDC-more-turb) that predicted both the temperature and the methane concentrations better than in the previously analyzed runs. In this run, we added an extra source term in the transport equation for the kinetic energy of turbulence. The source was active only in the fuel (methane) jet. This is indeed an ad hoc modification and as such is unjustified in the steady-state calculations. In our opinion, there are strong indications that modeling of the strong jet-weak jet interactions would require a model that should account for the enhanced entrainment of oxygen and enhanced rate of fuel combustion due to the non-stationary behavior of the weak (methane) jet. Interestingly enough,

running the NO_x postprocessor, after improving the temperature and methane concentration predictions in the weak (methane) jet, did not result in changes in the predicted furnace exit NO emissions, as reported in Table 2. The NO source, in terms of its location and magnitude, remained unaltered since the peak in-furnace temperatures remained the same.

Conclusions

Steady-state numerical simulations of a 0.58 MW burner that operated in a flameless oxidation mode have been carried out. Three combustion models have been tested:

- Eddy-break-up model with a two-step reaction scheme
- Eddy dissipation concept model with chemical equilibrium
- pdf/mixture fraction model with equilibrium, non-adiabatic look-up tables

The nitric oxide formation has been investigated with two different NO_x models both considering thermal and prompt NO_x formation. In one of the NO_x models the NO-reburning mechanism has been included. The model results have been compared both with the in-furnace measurements (including temperature, gaseous species, velocity, radiative heat flux) and with the furnace exit parameters. The following has been concluded:

1. With the exception of the small region located within the natural gas jet, the computations have resulted in predictions of good quality. The computed NO_x emissions have been in very good agreement with the measured values for a number of combustion-model/NO_x postprocessor combinations.
2. The NO_x is formed in an elongated, thin shear layer located between the natural gas jet and the air jet. To obtain good quality NO_x emissions predictions, it was enough to predict correctly the time-mean temperature and oxygen concentrations in this (flamelet) region. The subsequent application of the β-pdf function either to the temperature or to the mixture fraction resulted in correctly predicted NO_x emissions.
3. The NO_x is formed mainly by the thermal path. The prompt NO is of little importance. The NO-reburning mechanism is negligible in the analyzed case,
4. There are strong indications that non-stationary behavior of the weak (fuel) jet must be accounted for to improve the predictions within the jet.

REFERENCES

1. Katsuki, I. M., and Hasegawa, T., *Proc. Combust. Inst.* 27:3135–3146 (1998).
2. Weber, R., Verlaan, A. L., Orsino, S., and Lallemant, N., *J. Inst. Energy* 72:77–83 (1999).
3. Wünning, J. A., and Wünning, J. G., *Prog. Energy Combust. Sci.* 23(12):81–94 (1997).
4. Hardesty, D. R., and Weinberg, F. J., *Combust. Sci. Technol.* 8:201–214 (1974).
5. De Joannon, M., Langella, G., Beretta, F., Cavaliere, A., and Noviello, G., *Combust. Sci. Technol.* 153:33–50 (2000).
6. Nakamachi, I., Yasuzawa, K., Miyahata, T., and Nagata, T., *Apparatus or Method for Carrying out Combustion in a Furnace,* U.S. Patent 4, 945, 841, 1990.
7. Sobiesiak, A., Rahbar, S., and Becker, H. A., *Combust. Flame* 115:93–125 (1998).
8. Ishi, T., Zhang, C., and Sugiyama, S., "Numerical Analysis of NO_x Formation Rate in a Regenerative Furnace," in *Joint Power Generation Conference,* ASME EC-Vol. 5, 1997, pp. 267–278.
9. Hino, Y., Zhang, C., Ishii, T., and Sugiyama, S., "*Comparison of Measurements and Predictions of Flame Structure and NO_x Emissions in a Gas-Fired Furnace,*" AIAA/ASME Joint Thermophysics and Heat Transfer Conference, 1998.
10. Coelho, P. J., and Peters, N., *Combust. Flame* 124:503–518 (2001).
11. Pasenti, B., Evrard, P., and Lybaert, P., "*NO_x Production and Radiative Heat Transfer from an Autoregenerative Flameless Oxidation Burner,*" The Fourth International Symposium on High Temperature Air Combustion and Gasification, Rome, November 26–30, 2001.
12. Orsino, S., Weber, R., and Bollettini, U., *Combust. Sci. Technol.* 168:1–34 (2002).
13. Peters, A., and Weber, R., *Combust. Sci. Technol.* 110–111:67–101 (1995).
14. Magnussen, B. F., and Hjertager, B. H., *Proc. Combust. Inst.* 17:719–729 (1978).
15. Magnussen, B. F., "*On the Structure of Turbulence and a Generalized Eddy Dissipation Concept for Chemical Reaction in Turbulent Flow,*" Nineteenth AIAA Aerospace Meeting, AIAA, New York, 1981.
16. Brink, A., Hupa, M., Breussin, F., Lallemant, N., and Weber, R., *AIAA J. Propul. Power* 16(4):609–614 (2000).
17. Chen, W., "A Global Reaction Rate for Nitric Oxide Reburning," Ph.D. thesis, Brigham Young University, Salt Lake City, Utah, 1994.
18. De Soete, G. G., *Proc. Combust. Inst.* 15:1093–1102 (1974).
19. Hanson, R. K., and Salimian, S., "Survey of Rate Constants in H/N/O Systems," in *Combustion Chemistry,* 1984, p. 361.

COMMENTS

Bassam Dally, University of Adelaide, Australia. I'd like to comment that I measured similar flames and found that finite-rate chemistry is important and hence the model you used may not be applicable. It seems to me that the initial conditions at the jet exit may contribute to the discrepancy. Can you comment on that? Do you think that including radiation in your model will improve your predictions?

Author's Reply. Two years ago, we also thought that the finite-rate chemistry might be important [1]. As for today, after carrying out further computations (Ref. [12] in paper), we understand that the finite-rate chemistry cannot be responsible for such large differences between the measured and predicted properties of the natural gas jet. The uncertainties in the inlet conditions of the jet are not responsible for these differences. In our numerical simulations, we use the ordinate transfer radiation method. The absorption coefficients are calculated spectrally or using a gray gas approximation. In either case, the radiation alters the temperatures in the natural gas jet by 30–50 °C, while the observed discrepancies are substantially larger. As we now understand the problem, the non-stationary behavior of the weak natural gas jets is responsible for the discrepancies.

REFERENCE

1. Weber, R., Orsino, S., Lallemant, N., and Verlann, A., *Proc. Combust. Inst.* 28:1315 (2000).